Applied Mathematical Modelling 88 (2020) 266–282

Contents lists available at ScienceDirect

Applied Mathematical Modelling

journal homepage: www.elsevier.com/locate/apm

A network model for stemflow solute transport

Amy Tucker[a], Delphis F. Levia[b,*], Gabriel G. Katul[c], Kazuki Nanko[d], Louis F. Rossi[a]

[a] Department of Mathematical Sciences, University of Delaware, Newark, DE, USA
[b] Departments of Geography & Spatial Sciences and Plant & Soil Sciences, University of Delaware, Newark, DE, USA
[c] Nicholas School of the Environment & Department of Civil and Environmental Engineering, Duke University, Durham, NC, USA
[d] Department of Disaster Prevention, Meteorology and Hydrology, Forestry and Forest Products Research Institute, Tsukuba, Ibaraki, Japan

ARTICLE INFO

Article history:
Received 2 March 2020
Revised 12 June 2020
Accepted 21 June 2020
Available online 2 July 2020

2010 MSC:
00-01
99-00

Keywords:
Bark
Furrow
Leaching
Network
Stemflow

ABSTRACT

While the role of stemflow in directing and concentrating water and nutrients at the tree base is rarely in dispute, its mathematical representation remains a subject of inquiry and research. A network model that seeks to estimate stemflow solute concentration and leaching is proposed. The model accommodates the physico-chemical properties of individual furrows embedded within the tree bark and their interconnections. The within-furrow equations for water and solute transport that include leaching are first developed and integrated along a rough-bark network topology to describe solute concentration and fluxes out of the network. The model is parameterized using published data on stemflow, field measurements of bark geometry, and laboratory experiments on bark leaching for potassium, magnesium, and calcium. The parameterization is intended to impose plausibility constraints and not to test model predictions at a particular site, a single event, or an individual experiment. The outflow concentration is then analyzed as a function of the network complexity that includes asymmetry in the lengths or subpaths connecting network nodes. For a symmetric network, an effective 'channel-flow' analogy may be used to represent solute concentration at the outflow. However, as the asymmetry increases in subpath lengths, the efficiency of the bark network at moving solutes diminishes for the same rainfall input onto the stem. The network representation featured here is by no means offering a 'finality' to the stemflow mathematical representation. It must be viewed as an embryonic step that opens up the possibility of using modern advances in network theories to link rainfall properties to stemflow water and solute input from a variety of tree species with differing bark microrelief configurations into the soil.

1. Introduction

Stemflow, the water that flows over the exterior of a plants trunk or stem, represents a fraction of the intercepted precipitation directly striking the trunk or converging as branchflow onto the trunk. Even when stemflow constitutes less than 2% of the gross incident rainfall, it almost always funnels more water per unit area to the base of the stem than either rainfall or throughfall alone [1]. Hence, its role in directing and concentrating water and nutrients from the canopy into the soil-root system can be substantial, yet understudied when compared to many hydrological fluxes. Perhaps this 'lag'

* Corresponding author.
E-mail address: dlevia@udel.edu (D.F. Levia).

https://doi.org/10.1016/j.apm.2020.06.047
0307-904X/

in stemflow studies relative to other hydrological fluxes is not entirely surprising. While stemflow and concomitant solute transport can be described using the Navier-Stokes equations, implementing these equations along the channel network within the bark remains a formidable task. Any upscaling of these point-equations to arrive at stemflow fluxes, even from a single tree, requires coarse graining non-linear and multi-scaled transport processes whose basic properties are rarely measured. However, the time is ripe to begin confronting these challenges given the rapid progress in measurements and in theories dealing with transport and chemical transformation in physical and biological networks [2–6].

For some rough-barked tree species, water collected from a tree crown is transmitted onto a complex network of ridges and furrows distributed along the bark. This water collection mechanism is impacted by canopy structure [7,8] such as branch number and branch inclination angle. Branch inclination alone was found to be a key factor affecting the quantity of branchflow onto the stem. Some studies reported that about 80% of the impacting rainfall is being channeled as branchflow when branch inclination angles exceed 60° above the horizontal [9]. In addition, the funneling effect of branches was greater once branches were wet [9] suggesting that both intrastorm rain dynamics and antecedent hydroclimatic conditions play a significant role [10–13]. Once collected, the water and solutes are then transported through the bark via a network of interconnected ridges and furrows that can be hydrodynamically rough, smooth, or transitional. In a single furrow, water flow responds to a number of forces including gravitational, frictional (viscous or turbulent), and under some conditions, surface tension. The flow depth within the furrow may be small so that the flow resembles a porous medium, partially full (resembling free surface flow) or overflowing (gravitational free-fall). The geometric properties of each furrow (e.g. their length, angle, effective width, micro-roughness, and chemical properties) also vary along the bark, necessitating information that is rarely collected in hydrological and ecological studies. Moving beyond the single furrow scale, connections between multiple furrows within the bark and ridges also impose extra constraints that alter its 'aggregate' behavior in ways that remain to be explored and partly motivate the model development here.

With regards to biogeochemical cycling, it has been shown that annual nutrient returns to forest soils for elements such as potassium and sulfur is predominantly via throughfall and stemflow instead of litterfall [14]. Some studies [15] found differences among canopy-only stemflow, stem-only stemflow, and canopy-and-stem stemflow indicating that differential routing and transport through the canopy can affect stemflow chemistry. A greater diversity of bacteria occur on the bark than leaf surfaces [16] and stemflow has been documented to transport atmospherically deposited dryfall and tree-derived leachates to the tree base [17]. Thus, progress on stemflow in hydrology and biogeochemistry cannot ignore coupling between flow dynamics and solute transport.

Motivated by these knowledge gaps on the physico-chemical dynamics of stemflow, the goal here is to evaluate a network model representation that minimally seeks to estimate stemflow solute fluxes for various network complexities. Clearly, accommodating all aspects and path details of stemflow dynamics along with solute transport is well beyond the scope of a single study. Hence, the emphasis is on processes and mechanisms likely to be common for stemflow representation of some rough-barked tree species. For this reason, the focus is on the 'channelization' effects within and over the bark furrows and its influence on washoff and leachate dynamics of solutes for events of heavy rain intensities. The work here does not explicitly consider the actual collection mechanisms from foliage and branches and assumes the flow rate and chemical fluxes at the upper most section of the bark is predetermined or externally supplied. More precisely, this modeling effort is focused on comparing stemflow solute leaching and transport between single-path and multiple-path (i.e., network) scenarios. Even within this restricted scope, numerous assumptions and simplifications must be made when describing water and solutes through the bark network. The proposed model does accommodate several (but not all) processes highlighted in the introduction thereby making it suitable for both - diagnostic and prognostic purposes. Such a model is also intended to be used in generating competing hypotheses about connections between the network properties and the physico-chemical properties of the bark. It is also envisaged that a network representation of stemflow may enlighten the role of plant stem on biogeochemical cycling in forests at longer time scales.

2. The model

Stemflow is assumed to occur within a network of connecting furrows embedded in the tree bark. Throughout, the flow network is approximated by a directed graph characterized by edges that represent uninterrupted furrow and nodes as shown in Fig. 1. For convenience, nodes are indexed with integers and an edge connecting node i and node j is denoted e_{ij}. When a furrow ends, it is assumed that water traveling down the furrow will cross the ridge vertically and join the next furrow directly below it. Hence, to describe stemflow and concomitant solute concentration, it is necessary to first describe governing equations in a single furrow as a continuum [18], and then 'upscale' the outcome to the network level. For this reason, the model development is divided into two general parts. The first part reviews the governing equations describing the bulk velocity and solute concentration within a single furrow. The second part discusses minimal features of the network topology connecting furrows, which then serves as the spatial integrating kernel for the single furrow equations to arrive at water and solute fluxes out of the bark and into the soil. While stemflow is not solely restricted to furrows of rough-barked trees, this study specifically focuses on the network modeling of stemflow in furrows that manifest in a variety of shapes and sizes on different tree species (Fig. 1). Since this work is the first instance where stemflow is described using a network, the role of network symmetry/asymmetry and its impacts on macroscopic features pertaining to solute outflow from stems is a logical first step.

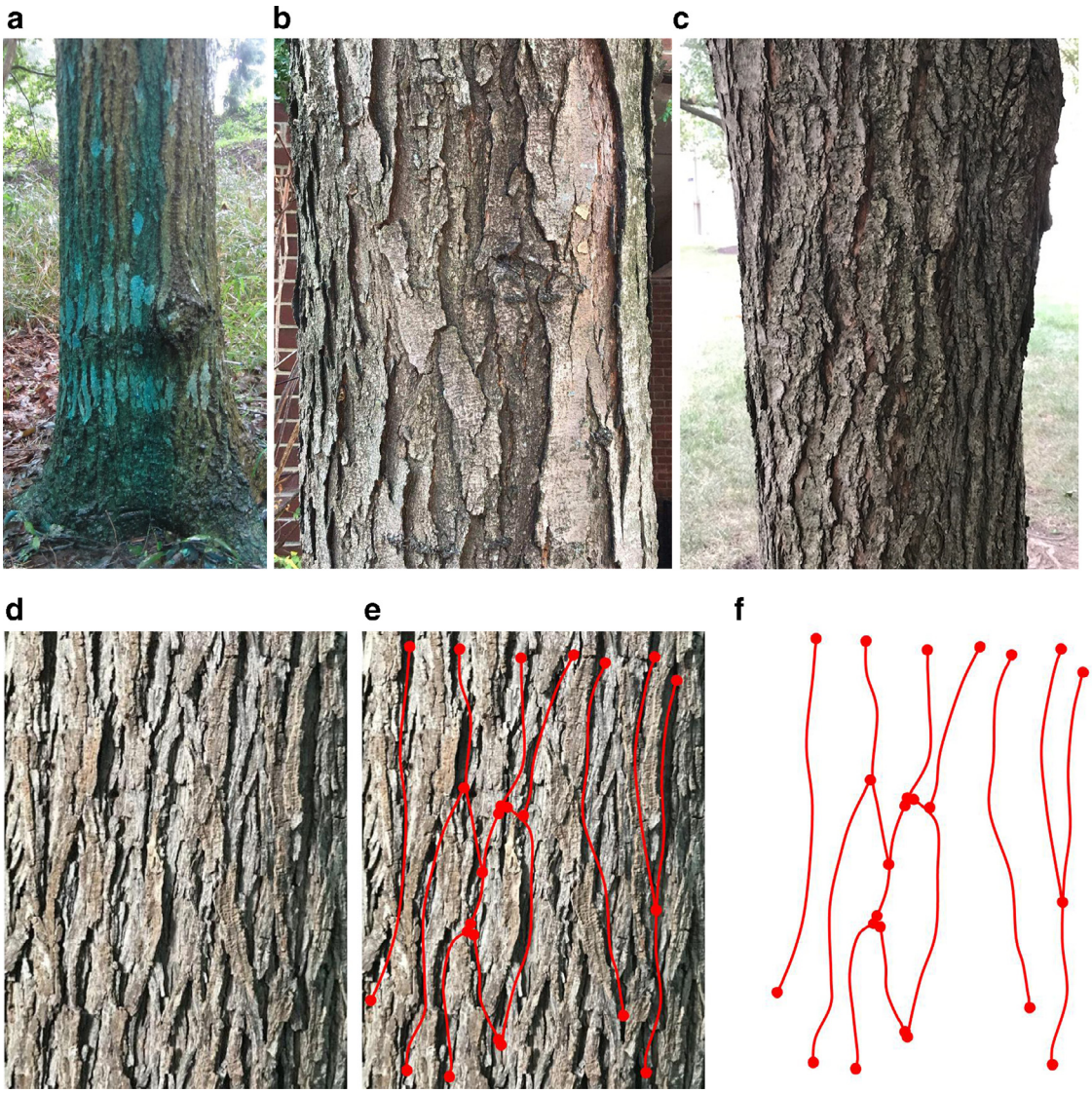

Fig. 1. Rough-barked trees species with different bark microrelief configurations and ridge-furrow patterning, (a)–(d). The network model for stemflow solute transport developed covers furrows (see Suppl. Material, S1) regardless of ridge-furrow configuration. (a) *Quercus serrata* Murray (konara oak); the removal of blue dye (applied before a rain event) identifies areas on the tree stem where stemflow occurred over ridges and in furrows (photo credit: N. Imamura) described elsewhere [19]; (b) *Gleditsia triacanthos* L. (honey locust) (photo credit: D.F. Levia); (c) *Acer rubrum* L. (red maple) (photo credit: D.F. Levia); (d) *Carya tomentosa* (Lam.) Nutt. (mockernut hickory) (photo credit: D.F. Levia) is another example of a rough-barked tree (i.e. a bark that exhibits a range of microrelief, becoming furrowed with age) that is to be used for illustration throughout this work. This mid-aged tree has a diameter at breast height of 0.493 m. Mapping bark geometry to a directed graph, (e) and (f). All edges are directed downward. (e) some furrows are traced in this section of the tree stem. When a furrow ends, the tracing extends over the ridge immediately below the dead end. (f) the resulting network is a directed graph with water entering from the nodes at the top and departing from the nodes at the bottom. The resulting network, extending over the whole tree stem, is composed of a sequence of patterns including isolated paths (i.e. single lines) and connected paths (multiple lines converging and diverging from nodes) with variable number of connections. Canonical patterns resembling these individual sequences are used in model calculations but the precise geometric scaling of the interconnected furrow dimensions is not matched. (For interpretation of the references to color in this figure legend, the reader is referred to the web version of this article.)

The following assumptions guide the model development:

1. All flow travels through furrows in the tree bark. If the furrow ends, it is assumed that flow travels vertically downward over the intervening ridge to the next furrow.
2. The flow in furrows is free-surface gravity driven, meaning that surface tension effects and splashing from rain is momentarily ignored.
3. The flow is established along the furrows and maintains its connectivity. Depending upon the rain intensity and tree type, connected flow paths can be established in minutes to as much as an hour.

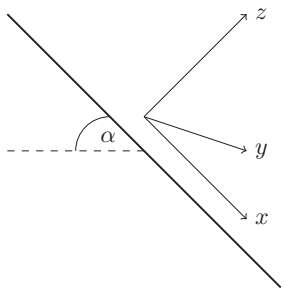

Fig. 2. Coordinate system for water flow on an inclined furrow at angle α.

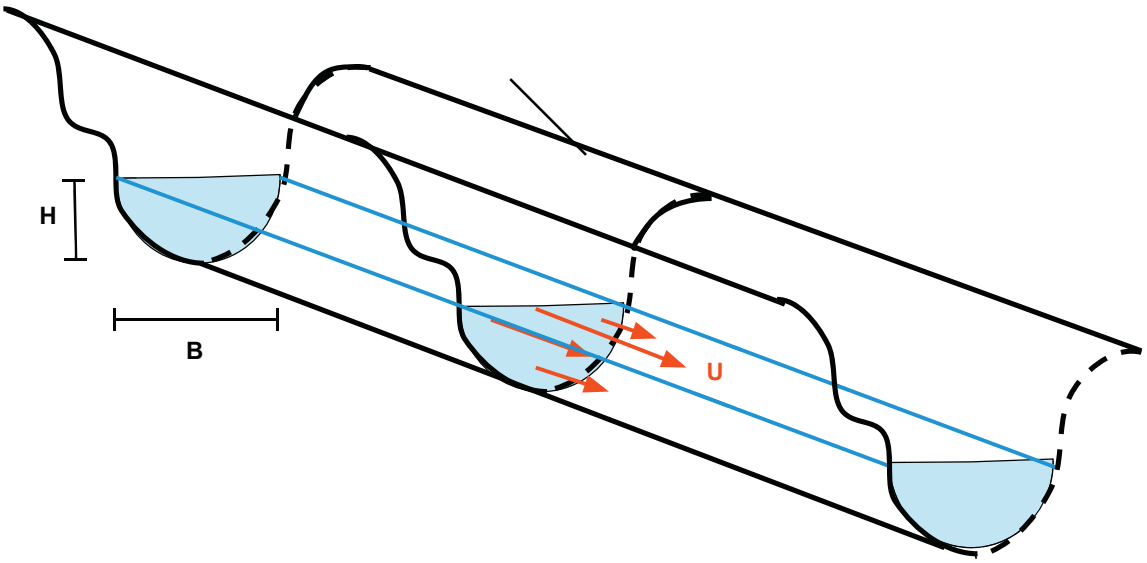

Fig. 3. Flow geometry in a single furrow. The water depth within the furrow (H) and the effective furrow width (B) are shown. Note that H is assumed to be smaller than the furrow depth.

2.1. Water flow in a single furrow

It is assumed that the flow occurs in an inclined furrow characterized by an angle α from the horizontal. The coordinate system is shown in Fig. 2 and the flow geometry is featured in Fig. 3. That is, the x-direction defines the direction of the flow within the furrow or the longitudinal direction, the y-axis defines the lateral direction, and the z-axis is the direction orthogonal to the furrow base. Three geometric variables are now defined: The cross sectional area A_c or the area normal to the flow, the wetted perimeter P_w (i.e., the perimeter of A_c that is wet and in contact with the furrow wall), and the furrow length l along the x direction. For this flow geometry and since the interest is in bulk (or area-averaged variables), the simplified one-dimensional continuity equation along the x-direction for water flow is given by

$$\frac{\partial A_c(x,t)}{\partial t} + \frac{\partial Q(x,t)}{\partial x} = S_w(x,t), \tag{1}$$

where t is time, Q is the volumetric flow rate, and S_w are the water sources and sinks that can include evaporation of water from the furrow, direct rain onto the furrow, and absorption and subsequent storage of water by the wood. Unless otherwise stated, all symbols to be used are defined in Tables 1 and 2. The derivation of Eq. (1) assumes that water flow is incompressible with a constant density ρ. A major simplification adopted now is to ignore the storage term in the furrow $(\partial A_c/\partial t)$ thereby ensuring steady-state conditions. Water storage capacities within the furrow can affect stemflow yield and subsequent solute fluxes depending on bark properties [20]. However, a logical starting point is to explore the steady-state conditions prior to any inclusion of the transient dynamics in water movement requiring bark-specific storage capacities. Likewise, S_w is also ignored meaning that (i) local evaporative losses, (ii) direct precipitation onto the free water surface within the furrow, and (iii) any absorption or release of water from the furrow wood is ignored. For steady flow in the absence of S_w, the continuity equation leads to a constant Q within a single furrow, which is to be determined from boundary conditions on the network (later described). The bulk velocity u in a single furrow can now be defined as $u = Q/A_c$. The main force driving water along the furrow is $(\rho A_c l)g\sin(\alpha)$, where g is the gravitational acceleration. The resisting force is

Table 1
List of symbols (English).

a_w	constant determined from furrow geometry
A_c	cross sectional area of a furrow
B	total base width of a furrow section
c	relative concentration in a furrow, $(q - q_R)/q_R$
C_d	drag coefficient, u_*^2/u^2
D, D_d, D_m	total diffusion, dispersion, and molecular diffusion coefficients, $D = D_m + D_d$
Da	Damköhler number, $[\gamma A_c l]k_c/(uA_c q_R)$
ø	Diameter of a tree at breast height
e_s	mean protrusion of height into the water by furrow micro-roughness
f	Darcy-Weisbach friction factor, $8C_d$
$f(q)$	solute leaching rate occurring across P_w
Fr	Froude number
g	gravitational acceleration
g_f	section factor for determining D_d
H	depth of water in a furrow
J	solute mass flux in a furrow from positions $x = a$ to $x = b$, $a < x < b$
k_c	constant transport rate with units of mass flux
l	furrow length in x direction
l_c	characteristic length scale in D_d
n	order of transformation reaction in $f(q)$
N_f	the total number of networks that can be packed onto the bark circumference of a tree
Pe, Pe_a	Péclet numbers in lateral and axial directions, ul_c/D_m, ul/D
P_w	wetted perimeter of a furrow
q, q_R	solute concentration and maximum solute concentration near saturation
Q	volumetric flow rate in a single furrow
r	half-width of the furrow section, $B/2$
Re_b	bulk Reynolds number, uR_h/ν
R_h	hydraulic radius, A_c/P_w
u	bulk velocity in a single furrow, Q/A_c
u_*	friction velocity, $(\tau/\rho)^{1/2}$
S_w	water sources and sinks
V	volume of water surrounding bark in the leaching experiment
x'	relative horizontal position along furrow, x/l

Table 2
List of symbols (Greek).

α	angle from horizontal by a furrow
β	constant used in building sample networks to control symmetry in furrows
δV	fixed water sample volume in leaching experiment
γ	inverse of the hydraulic radius, $P_w/A_c = R_h^{-1}$
λ	arises in the solution of Eq. (17), $\sqrt{\mathrm{Pe}_a \mathrm{Da}(\frac{\mathrm{Pe}_a}{\mathrm{Da}} + 4)}$
ν	kinematic viscosity of water
ρ	water density
τ	uniformly distributed stress on the area $P_w \times l$

assumed to originate only from wall friction characterized by a uniformly distributed stress τ acting upon an area formed by the wetted perimeter and furrow length ($=P_w \times l$).

For steady and uniform flow, the local and advective acceleration terms can be ignored and these two forces (i.e. friction and gravitational) are in balance leading to a kinematic representation of τ given by [21,22]

$$u_*^2 = \frac{\tau}{\rho} = \frac{A_c}{P_w} g \sin(\alpha), \tag{2}$$

where $u_* = (\tau/\rho)^{1/2}$ is the friction velocity and the quantity $R_h = A_c/P_w$ is the hydraulic radius. If the flow is experiencing finite acceleration (local and advective), then Eq. (2) must be replaced with the so-called Saint-Venant (or shallow water) equations [23] discussed elsewhere [24]. To determine u, a link to u_* is now required and can be operationally achieved using a drag coefficient C_d defined here as $C_d = u_*^2/u^2$. With this representation, the well-known Chezy equation can be recovered and is given by [22,25]

$$u = C_d^{-1/2} \sqrt{R_h g \sin(\alpha)}. \tag{3}$$

It is to be noted that up to this point, Eq. (3) applies to both laminar and turbulent flow states within the furrow. The distinction between these two flow states is based on how the bulk Reynolds number $Re_b = uR_h/\nu$ impacts C_d or a related quantity – the Darcy-Weisbach friction factor $f = 8\ C_d$ [26–29], where ν is the kinematic viscosity of water. The factor 8 arises from the definition of mean wall stress in pipes and is conventionally maintained when relating a bulk drag

coefficient to f in open channels. For small Re_b (laminar flow), $f = a_w Re_b^{-1}$ [28,30] and Eq. (3) reduces to

$$u = \frac{1}{a_w}\frac{g}{\nu}R_h^2 \sin(\alpha), \tag{4}$$

where a_w only depends on the section geometry. For circular sections and based on the definition of Re_b here, $a_w = 2$ whereas for a wide channel, $a_w = 3$. Operationally, the flow rate Q within a furrow is predetermined from water balance considerations within the network and what is sought is the water level (or A_c) and u. Combining $Q = A_c u$ with Eq. (4) leads to an algebraic expression given as

$$A_c R_h^2 = a_w Q \frac{\nu}{g\sin(\alpha)}, \tag{5}$$

where the right-hand side quantity is known. For a given furrow section geometry, A_c and R_h can be uniquely related to the water depth H within the furrow thereby allowing Eq. (5) to be solved for the single variable H. Once H is solved for, A_c and $u = Q/A_c$ can be readily determined. For illustration purposes, if the cross-sectional area in Fig. 3 is approximated by a wide rectangle of known width B (derived from furrow geometry) and unknown water depth H with $H/B << 1$, then Eq. (5) reduces to

$$H = \left[\frac{Q}{B}\frac{3\nu}{g\sin(\alpha)}\right]^{1/3}, u = \frac{Q}{BH} = \left[\left(\frac{Q}{B}\right)^2 \frac{g\sin(\alpha)}{3\nu}\right]^{1/3}, \tag{6}$$

where a_w was set to 3.

It will be remiss if a number of features about the canonical structure of these flow equations are not pointed out. To begin with, Eq. (4) can be re-arranged and expressed in non-dimensional form to yield Eq. (7)

$$Fr^2 = \frac{u^2}{gR_h} = \left[\frac{\sin(\alpha)}{a_w}\right] Re_b, \tag{7}$$

where Fr is a Froude number that is formed by the ratio of the flow inertia to the external field (gravitational here). Hence, the bulk laminar flow in a furrow can be reduced to a relation between two dimensionless numbers: the Froude number and the Reynolds number with geometric properties of the furrow acting as a scaling coefficient for this relation. Another interesting feature is that when setting $R_h = A_c/P_w = Q(uP_w)^{-1}$, Eq. (4) can be expressed as

$$u = \frac{1}{(a_w P_w^2)^{1/3}}\left[\frac{g}{\nu}Q^2\sin(\alpha)\right]^{1/3}. \tag{8}$$

This outcome is identical to an exact solution derived from the Navier–Stokes equations presented elsewhere [31,32] when ignoring local and advective acceleration terms, and area-averaging the point-wise velocity. Last, the derivation here can be extended to turbulent conditions, whether be they smooth, transitional, or fully rough [33] – provided the dependency of f on Re_b and relative roughness e_s/R_h is considered [22], where e_s is the mean protrusion height into the water by the furrow micro-roughness assumed to be uniformly distributed along P_w.

2.2. Solute transport in a single furrow

The conservation of solute mass is used to derive an equation for solute transport in the furrow. A unidirectional flow is assumed so that the variation in solute concentration q in the spanwise direction is small relative to variation in the streamwise direction. The exact conservation of solute over any interval $a < x < b$ then dictates that

$$\frac{d}{dt}\int_a^b A_c(x)q(x,t)dx + A_c(b)J(b,t) - A_c(a)J(a,t) = \int_a^b f(q)P_w(x)dx, \tag{9}$$

where J is the solute mass flux from positions $x = a$ to $x = b$, $f(q)$ is the solute leaching flux occurring across P_w that depends on the local concentration. Provided a and b remain constant in time, Eq. (9) reduces to

$$\int_a^b \left[A_c(x)\frac{\partial q}{\partial t}dx + \frac{\partial}{\partial x}(A_c(x)J) - f(q)P_w(x)\right]dx = 0. \tag{10}$$

Expression (10) is true for any choice of a and b. Under the mild assumption that the integrand is continuous yields an evolution equation for q along a furrow given by its common form

$$A_c(x)\frac{\partial q}{\partial t} + \frac{\partial}{\partial x}(A_c(x)J) = P_w(x)f(q). \tag{11}$$

While this representation of q enables describing what happens in a furrow with streamwise geometric variations, it will be further simplified so that network effects can be conveniently examined.

As with the water flow case, steady-state conditions are assumed (i.e. $q(x,t) = q(x)$ and $J(x,t) = J(x)$) and that the furrow has uniform cross-sectional geometry ($A_c(x) \equiv A_c$ and $P_w(x) \equiv P_w$), the basic model for transport along a single furrow reduces to,

$$\frac{\partial J}{\partial x} = \gamma f(q), \tag{12}$$

where $\gamma = P_w/A_c = R_h^{-1}$ is the inverse of the hydraulic radius. If the furrow is a wide rectangular section, then $\gamma = 1/H$ whereas for a cylindrical furrow flowing half-full ($H = r$), $\gamma = 2/r$ where r is the radius of the cylinder.

The solute flux J is given by its conventional form - an advective and dispersive transport term expressed as

$$J = uq - D\frac{\partial q}{\partial x}, \tag{13}$$

where D is the total diffusion coefficient that includes both molecular (D_m) and dispersive (D_d) contributions (i.e. $D = D_m + D_d$). The dispersive term arises due to area-averaging of an inhomogeneous velocity field. For laminar flow conditions, the dispersive contributions to J are dominated by the well-studied Taylor dispersion given by [2,34]

$$\frac{D_d}{D_m} = g_f Pe^2, \tag{14}$$

where $Pe = ul_c/D_m$ is a radial or vertical Peclet number measuring the advective to diffusive transport, l_c is a characteristic length scale (radial or vertical), and g_f is a factor that depends on the cross-sectional geometry. The original Taylor dispersion in tubes yields $l_c = r$ (the pipe radius) and $g_f = 1/48$. In open channels, $g_f = 2/105$ and $l_c = R_h$ or H for a wide rectangular channel [35]. For turbulent flows, the dispersion coefficient $D_d = \alpha_d R_h u_*$ [36,37], where α_d depends on the geometry ($\alpha_d \approx 10$ for wide open channels) and u_* can be inferred from Eq. (2).

With regards to the function $f(q)$, a model of maximum simplicity that includes only leaching is employed and is given as

$$f(q) = k_c\left(1 - \frac{q}{q_R}\right)^n, \tag{15}$$

where k_c is a constant having units of mass flux, n is the order of the transformation or reaction, and q_R is the maximum solute concentration near saturation. For $n = 0$, leaching is a constant input process whereas for $n = 1$, leaching is a first-order generation process.

For $n > 1$, the $f(q)$ resembles higher-order reactions that may be encountered in heterogeneous chemical systems due to presence of chemical segregation or blockage of some distant molecules to accessing the depositing surface. The most applicable model for the leaching of potassium and other substances of interest (e.g. calcium, magnesium) in stemflow is a binding/unbinding process with $n = 1$ [38]. With these approximations, a single second-order ordinary differential equation describes q along x and is given by

$$D\frac{d^2q}{dx^2} - u\frac{dq}{dx} + \gamma k_c\left(1 - \frac{q}{q_R}\right)^n = 0. \tag{16}$$

Eq. (16) can also be made dimensionless by defining the following variables: relative horizontal position $x' = x/l$ along the furrow length l, relative concentration $c = (q - q_R)/q_R$, the longitudinal or axial effective Péclet number $\mathrm{Pe}_a = ul/D$ (different from Pe used in the determination of D so as to accommodate Taylor dispersion), and a type of a Damköhler number $\mathrm{Da} = [\gamma A_c l]k_c/(uA_c q_R)$ defining a reaction rate to advective mass transport. The quantity in the squared brackets represent the wetted surface area of the channel so that the numerator is a natural scale for the rate of solute production through leaching and the denominator is a natural scale for solute transport by advection. The dimensionless form of the solute continuity equation becomes [39,40]

$$\frac{1}{\mathrm{Pe}_a}\frac{d^2c}{dx'^2} - \frac{dc}{dx'} + \mathrm{Da}(-c)^n = 0, \tag{17}$$

where the focus is, again, on common values of n (=0,1). For $n = 0$,

$$c(x') = A + \mathrm{Da}\ x' + \frac{\overline{B}}{\mathrm{Pe}_a}\exp\left(\mathrm{Pe}_a\ x'\right), \tag{18}$$

whereas for $n = 1$,

$$c(x') = A\exp\left[\frac{x'}{2}(\mathrm{Pe}_a - \lambda)\right] + \overline{B}\exp\left[\frac{x'}{2}(\mathrm{Pe}_a + \lambda)\right], \tag{19}$$

with A and $\overline{B}$ are unknown coefficients to be determined using two boundary conditions at the edges of the furrow, and λ is given by

$$\lambda = \sqrt{\mathrm{Pe}_a\ \mathrm{Da}\left(\frac{\mathrm{Pe}_a}{\mathrm{Da}} + 4\right)}. \tag{20}$$

To provide realistic estimates of leaching parameters k_c and q_R, laboratory experiments were conducted on three solutes common in stemflow biogeochemistry: potassium (K^+), calcium (Ca^{2+}), and magnesium (Mg^{2+}). The laboratory experiments were conducted as leaching into still water ($u = 0$) from wood. The back side of the wood was coated with silicone sealant to prevent leachate losses from the bark interior. This piece of bark was first placed in purified, deionized water. We anticipate that the bark has some unbounded potassium, calcium, and magnesium on its surface and that these ions dissociate into the water on a much faster timescale than those that are leached. After the initial immersion, the bark will leach potassium, calcium, and magnesium into the water. Water samples were removed and analyzed to determine q at fixed time intervals t_i =2, 4, 6, 12, 24 and 48 hours. The area contributing to the mass exchange between the bark and the water (A_w) was also measured. The chemical solution was well mixed (i.e. $\partial q/\partial x = 0$) so that measured $q(t_i)$ was uniform in the entire volume of the water body V surrounding the bark section. Since water samples of fixed volume δV were sequentially drawn at fixed time intervals t_i for concentration measurements, $V(t_i)$ experiences a decremented jump every time a sample is taken. For instance, if the initial water volume is V_0, then $V = V_0$ for $0 \le t \le 2$ hours, $V = V_0 - \delta V$ for $2 \le t \le 4$ hours, $V = V_0 - 2\delta V$ for $4 \le t \le 6$ hours, etc. Because V is changing with each sampling time t_i and noting that $J = 0$ for the experimental setup here (by design), the scalar mass balance in Eq. (11) reduces to

$$\frac{d(V\ q)}{dt} = k_c A_w \left(1 - \frac{q}{q_R}\right)^n, \tag{21}$$

where k_c is the sought unknown transport rate in Eq. (16) to be experimentally determined, and q_R is now interpreted as the maximum solute concentration in water. When modeling this experiment, it is to be noted that the solute amount Vq is discontinuous because finite samples are being taken at discrete times. Similarly, the concentration q is a continuous function of time with jump discontinuities in dq/dt for the same reason. Eq. (21) can be expressed as

$$\frac{dq}{dt} = \frac{k_c A_w}{V}\left(1 - \frac{q}{q_R}\right)^n - \frac{q}{V}\frac{dV}{dt}, \tag{22}$$

where the last term $(q/V)(dV/dt)$ is a sum of δ – functions centered at sampling times t_i and is zero elsewhere. The ratio A_w/V is analogous to the aforementioned parameter γ but applied to the test vessel instead of a furrow. As a practical matter, q can be determined by solving

$$\frac{dq}{dt} = \frac{k_c A_w}{V}\left(1 - \frac{q}{q_R}\right)^n, \tag{23}$$

on each subinterval $[t_i, t_{i+1}]$ and imposing continuity of q at each t_i. Thus, for $n = 1$, Eq. (23) can be integrated between two consecutive sampling times t_i, t_{i+1} to yield the constraint,

$$q(t_{i+1}) = q(t_i)e^{-\frac{k_c A_w}{q_R V_i}(t_{i+1}-t_i)} + q_R\left(1 - e^{-\frac{k_c A_w}{q_R V_i}(t_{i+1}-t_i)}\right), \tag{24}$$

where $t_0 = 0$, $V_i = V_0 - i\delta V$ is the water volume at t_i. The experiment yielded six $q(t_i)$ measurements for $i = 1, 2, 3, 4, 5$ and 6, each satisfying Eq. (24). The $q(0)$ can be computed by extrapolation to $t = 0$ so as to estimate the initial unbound potassium, calcium, or magnesium on the bark surface that dissociates when the bark is immediately immersed into clear water. The two sought unknown quantities q_R and k_c can be solved from these six measurements by performing nonlinear least-squares fit to the $q(t_i)$ measurements.

The best fit result is shown in Fig. 4 illustrating the leaching properties of the bark for potassium. The best fitting procedure yielded optimal $k_c = 1.66 \times 10^{-1}$ mg cm^{-2} hr^{-1} and $q_R = 5.98$ mg l^{-1}. The same technique was applied to calcium ($k_c = 3.01 \times 10^{-2}$ mg cm^{-2} hr^{-1} and $q_R = 25.6$ mg l^{-1}) as well as magnesium ($k_c = 3.91 \times 10^{-2}$ mg cm^{-2} hr^{-1} and $q_R = 5.64$ mg l^{-1}). Again, the extrapolation of the fitted model to $t = 0$ provides an estimate of $q(0) > 0$.

Due to a greater reliance on ion exchange processes for divalent than monovalent cations [41], there was a weaker curvilinear fit for Ca^{2+} and Mg^{2+} when compared to K^+ for the duration of bark saturation. The initial higher concentration and then decline of calcium and magnesium concentrations was partly attributable to the washoff of unbound ions (between the first and second measurements) followed by the subsequent rising of calcium and magnesium concentrations as the ion exchange processes of bark leaching predominated. No such pattern was observed for potassium since it is primarily derived from leaching [17]. In all cases, the model with $n = 1$ agrees with experiments for all three scalars analyzed. These values for k_c and q_R with $n = 1$ are now used throughout to represent a plausible $f(q)$ for each furrow in the network. These measured bark leachate cation concentrations are within the range of actual stemflow leachate concentrations from other hardwood species [20,42] thereby providing some generality to the parameterization of $f(q)$.

2.3. Scaling up from furrow to network level

The water and solute transport equations must be solved in each furrow along the flow network embedded in the bark. Geometric parameters R_h, e_s, r, and l can vary from furrow to furrow. Chemical and flow parameters (i.e. k_c, q_R and u) also depend upon the furrow properties and the flow rate so they also vary from furrow to furrow. The sign of u depends upon the order of the indices because u represents flow velocity from node i to node j. As before, the particular solution for the transport equations along each furrow corresponding to edge e_{ij} is indicated with indices ij. For example, the solute

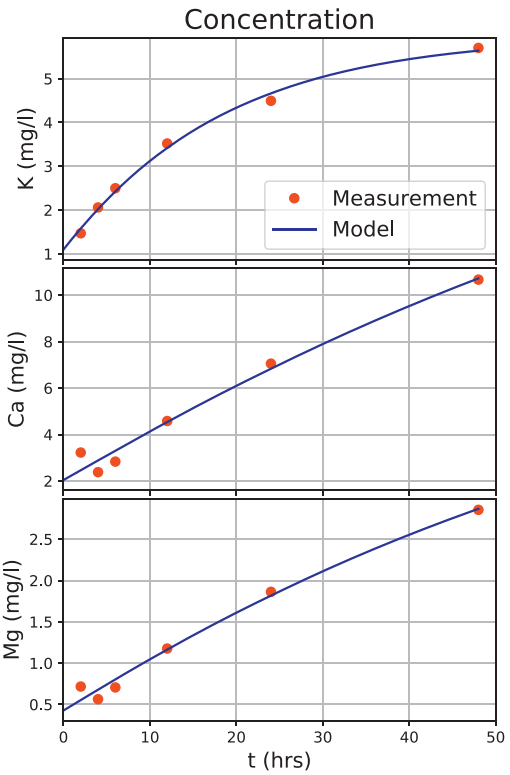

Fig. 4. Determining optimal parameters k_c and q_R by fitting Eq. (24) to the six potassium, calcium and magnesium concentration measurements. Root mean square errors (in concentration units) for the three model fits are 0.042, 0.175 and 0.038, respectively.

concentration along furrow e_{ij} is denoted by $q_{ij}(x)$. For network flow problems, boundary conditions are interdependent and complicate any upscaling from single furrow to stem.

Physical boundary conditions are applied at each node to formulate the mathematical boundary conditions necessary to solve the full system. In total, two boundary conditions for every edge are needed to determine the integration parameters A and $\overline{B}$ in the solute transport equation. At the 'top' of the network, that is the portion corresponding to the top of the stem, it is assumed that the inflow Q and the concentration (and subsequently the flux into the network) is known. At each node, the concentration at the end of every connected edge is the same (i.e. continuity requirements - no storage at the node). Likewise, the solute flux from the ends of all connected edges must sum to zero at a given node (i.e. what goes in leaves the node). This condition is necessary to conserve the total solute mass and is analogous to Kirchoff's Law for electric circuits. The total solute flux out of the right end of an edge ($x' = 1$) is defined to be

$$J = \left(uq - D\frac{dq}{dx} \right)\Bigg|_{x'=1}. \tag{25}$$

It is necessary to provide a boundary condition for each flow exit node. Applying appropriate outflow conditions is a challenging modeling and computational issue. In this case, the exact solution for q can be leveraged to determine appropriate Robin-type boundary conditions at outflow nodes. The key assumption is that if the length of an outflow edge were to be extended to infinity, no solute transport would be allowed to travel back into the domain. Another interpretation of such proposed outflow boundary condition is that it corresponds to a zero concentration gradient when $l \to \infty$. In other words, the system is *causal* and changing the length of an exit edge does not change the solution for very large l. The particular solution for a furrow with an exit node on one end would correspond to $B = 0$ in Eq. (19), where we only consider the $n = 1$ case from this point onward because it explains the data well. This is equivalent to applying the Robin condition at $x' = 1$ given by,

$$\frac{dc(1)}{dx'} - \frac{1}{2}(\mathrm{Pe}_a - \lambda)c(1) = 0, \tag{26}$$

assuming $x' = 1$ corresponds to an exit node. In the limit $l \to \infty$, this corresponds to $dc(1)/dx' = 0$. This condition amounts to one additional constraint per exit edge.

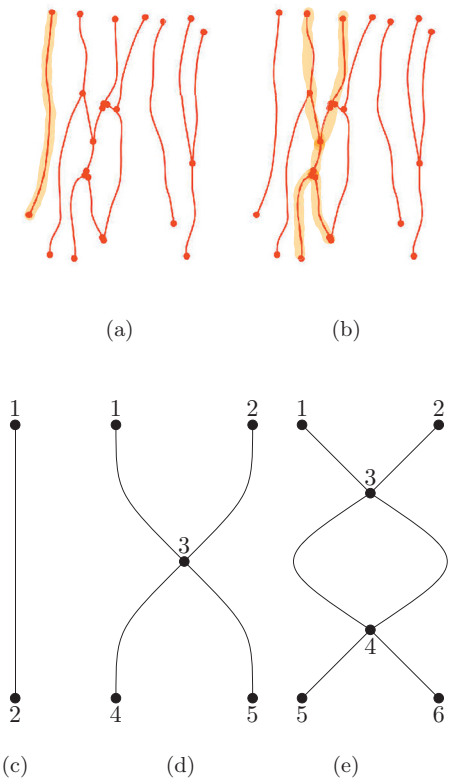

Fig. 5. Sub-networks from a furrow network in bark are used as example networks for the model (see Fig. 1). The simplest sub-network is a single channel, (a) and (c). A modestly more complex system is shown in (b) and (d). If two sub-networks of type (d) are stacked together, it yields sub-network (e). At left (d), all edges have a length of 10 m. At right (e), the top and bottom edges have length of 5 m while the center edges have a length of 10 m. Thus, both networks traverse 20 m.

3. Case studies for canonical networks of stemflow

Three case studies are presented to demonstrate the efficacy of the network model for stemflow with leaching of K^+. Two of the three examples come directly from *Carya tomentosa* bark (see Fig. 1(d)–(f)), and the third evokes a more complex network with asymmetry to represent mixing down a longer section of the tree stem. It can also be seen that these simple networks shown in Fig. 5 (c)–(e) represent sub-networks in an entire stemflow network. A repeating topology of sub-graphs like Fig. 5 (c)–(e) can be used to understand residence time and the impact of asymmetries through the complete stemflow network. Hence, instead of dealing with repeating topology, the sub-graph pattern will be used for the entire stem for illustration purposes. Such a representation does not preserve all aspects of the geometric complexity in the bark network, but it allows for broad conclusions to be drawn about symmetry breaking along the paths (as shown later). For simplicity, the furrows in these calculations are assumed to be rectangular with a constant width B though the approach allows for other geometry to be used.

Table 3 summarizes the parameter values used in the calculations. Measurements of the mockernut hickory tree bark shown in Fig. 1(d)–(f) were used to determine average furrow width (B) and height of 0.0056m and 0.01057m, respectively. The furrow α is chosen based on observation of the bark furrows though we note from inspection of Eq. (4) that the model is insensitive to this angle because stems are essentially vertical. The diameter at breast height (ø at 1.37m), routinely used as a characteristic diameter in forestry studies, was also measured for the same tree and found to be 0.493m. If the width between two channels is 0.0112 (= 0.0056 x 2)m so as to account for a furrow-ridge combination, the total number of networks that can be packed onto the bark circumference of this tree is

$$N_f = \frac{\pi\,(ø)}{2B} = \frac{3.14 \times 0.493}{2 \times 0.0056} \approx 140. \tag{27}$$

For a similar rough-bark species, a sample rainfall event of 25 mm per 18 hours generates, on average 174cm^3 per 5min and a peak of 980cm^3 per 5min in stemflow as measured and reported elsewhere [44]. Hence, the expected flow rate per furrow is about 2×10^{-8} m^3 s^{-1} at such a peak value. We selected a $Q = 4 \times 10^{-8}$ m^3 s^{-1} (i.e. double) to reflect more intense periods and/or higher rainfall intensities so as to amplify the significance of stemflow in the overall network. Yet, despite this higher intensity, the resulting u and H yield a furrow-scale Reynolds number (see Table 3) that is much smaller

Table 3
Table of measured and computed model parameters used in all network model calculations. Values above the double bar indicate accepted physical constants or direct measurements from the tree bark. Values below the double bar are computed from the values above the double bar.

g	9.8 m/s^2
ν	1.004×10^{-6} m^2/s
Q	4×10^{-8} m^3/s
α	88 (deg)
B	0.0056m
D_m from [43]	1.84×10^{-9} m^2 s−1
k_c	1.66×10^{-1} mg cm^{-2} hr^{-1}
q_R	5.98 mg l^{-1}
H	1.4×10^{-4} m
u	5.0×10^{-2} m/s
D	0.22 m^2/s
R_h	5.88×10^{-3} m
Pe_a	0.056
Da	99.9
Re	7

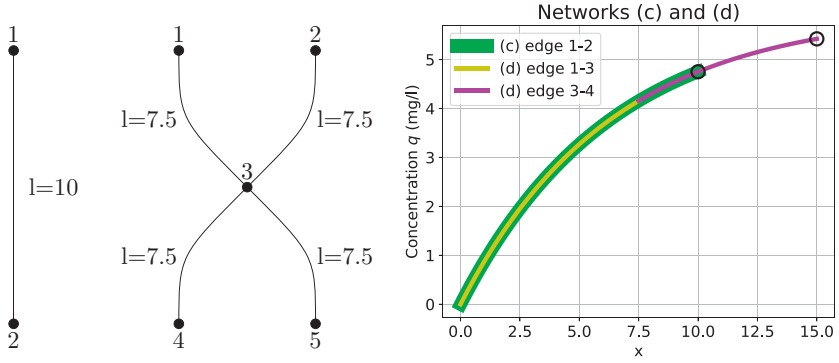

Fig. 6. The networks referred to in this figure are from Fig. 5. Example solutions over networks (c) and (d) representing typical pathways shown in panels (a) and (b) of Fig. 5. All lengths are measured in meters and concentrations are in mg/l. Network (d) is symmetric. The horizontal axis represents distance moving from top to bottom along a furrow. Since the network is symmetric, solutions along all paths are the same as evidenced by Eq. (28). To demonstrate the role of the overall length of the network, the edge lengths of network (d) are chosen so that the total distance from top to bottom is 1.5 whereas the network (c) has length 1. Black open circles indicate the final concentrations at the bottom of networks c (x=10) and d (x=15).

than the critical value for transitional or turbulent flows in open channels and pipes (>> 100). For this reason, the laminar solution linking Q to u or H as well as the Taylor dispersion formulation are employed throughout. In all the examples, the B and u are assumed to be uniform across the network. A non-uniform as well as transient solutions are possible but they are not discussed to maintain focus on the network configuration. The equations to be solved are all in steady-state, which requires a sufficiently long rainfall duration compared to any transient period prior to attainment of steady-state. Last, some objections may be raised about the use of differing data sources (i.e. not from the same site, species, tree, or even single event) to parameterize the furrow-scale flow and solute transport equations. Again, the goal here is only to use these data sources to arrive at a set of plausible parameters for the study of network topology. This parameterization is not intended to reproduce a particular experiment or data set.

In Fig. 5, two sample networks for model calculations are contrasted. An illustration of how the boundary conditions and the solute equations are combined and solved is featured in the appendix.

In the first example of a simple channel (network (c) in Fig. 5), the exact solution can be expressed analytically from Eq. (19), knowing that $c(0) = -1$ and that solutions must exponentially saturate to q_R as $x \to \infty$:

$$c(x') = -\exp\left[\frac{x'}{2}(\mathrm{Pe}_a - \lambda)\right]. \tag{28}$$

In fact, any of the networks (c), (d), and (e) will follow the same unique solution as long as the distance along all possible paths from top to bottom is the same. Mixing occurs at the nodes only if there are paths covering different distances. This point is illustrated in Fig. 6. The solutions over both networks collapse onto a single curve as expected and begin saturating at q_R. Since the overall length of network (d) is longer than network (c) in this example, water resides in the furrows longer so more leaching and increased concentration towards q_R occurs but following the same curve.

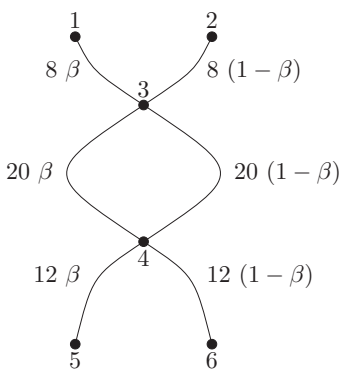

(a) Network (e) with varying edge lengths using parameter β. The representation shown has $\beta = 1/2$.

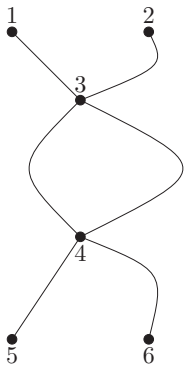

(b) Representation of the furrow network with $\beta = 1/4$.

Fig. 7. Representations of network (e) (see Fig. 5) with variable edge lengths. Path lengths affect the residence time of water within the furrows. In network (e), there are eight possible paths through the network from top to bottom. There are a total of 40 meters of furrow in the network, independent of β.

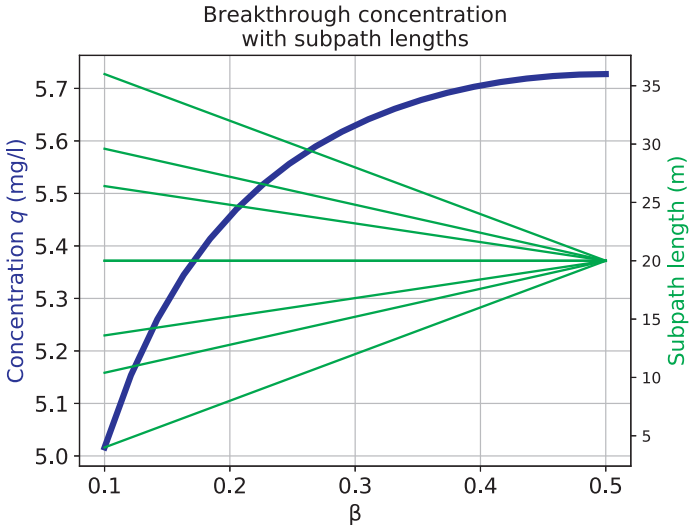

Fig. 8. Breakthrough or outflow concentration curve from network (e) as a function of asymmetry parameter β (see Fig. 7). The blue curve represents the average concentration from nodes 5 and 6. Each green line represents the length of one subpath through the network. (For interpretation of the references to color in this figure legend, the reader is referred to the web version of this article.)

Since mixing occurs at the nodes only if there are subpath differences, the edges of network (e) have been assigned different lengths as shown in Fig. 7. The parameter β is now used to vary the lengths of edges while keeping the total length of all the furrows in the network constant. As such, the degree of asymmetry in the subpaths can be controlled by varying β. In such a network, there are eight possible paths from top to bottom. In all these paths, there are seven different path lengths[1], which means there are seven different residence times. In Fig. 8, the mean concentration leaving nodes 5 and 6 (and entering the soil) is shown as a function of β and labelled as a 'break-through' curve. In the same figure, the individual path lengths are presented as green lines. For instance, the top line corresponds to the subpath following edges 2–3, 3–4 (right side), and 4–6 that has the longest length of the eight subpaths. The bottom line corresponds to the subpath following edges 1–3, 3–4 (left side), and 4–5, and it has the shortest length of the eight subpaths. While the network mixes solute at nodes 3 and 4, greater asymmetry decreases transport and lowers q at outflow points. Intuitively, this can be explained by the fact that difference between the solute concentration after traveling a distance l and full saturation is a quantity that decays exponentially, e^{-l} (for $n = 1$), so that the increases in furrow length and residence time have diminishing impact (with $q \to q_R$). The net output of two furrows with total length L is when each furrow has length $L/2$ for the simple reason that this value maximizes $e^{-x} + e^{L-x}$.

[1] The reason why there are not eight unique path lengths is that two of the paths must always be of equal length.

Fig. 9. A completely wetted *C. tomentosa* tree trunk following a heavy rain event (photo credit: D.F. Levia). Future iterations of the network model for stemflow solute transport will include stemflow occurring both within furrows and over ridges.

4. Conclusion

The network model developed here for rough-barked tree species represents a first attempt to unpack the 'black box' of solute transport along tree trunks. The model is formulated so as it accounts for laminar and turbulent flow within bark furrows and is able to capture solute leaching, concentration, and mass flux at any point along the network of interconnected and interlocking furrows and ridges. The single furrow equations identified that the bulk velocity, depth, and scalar concentration vary with 5 dimensionless quantities: Reynolds number, Froude number, a vertical and a longitudinal Péclet numbers, and a Damköhler number. Future model iterations also will account for ridge flow as both ridges and furrows leach solutes upon wetting (Fig. 9). Nonetheless, the network approach proposed here can be imminently used to develop reduced order models that interface with other approaches needed for describing soil biogeochemistry in forested ecosystems. By reduced order models, we mean models that replace the complex network of interconnected furrows and ridges with a bulk hydraulic quantity analogous to the effective single resistor-capacitor network in electric networks.

It is envisaged that this network model representation will spawn developments of various hypotheses about the connections and linkages among network properties and the physico–chemical properties of bark. The initial focus was purposely directed to the effects of symmetric and asymmetric relations (mainly distances between discrete junctions or nodes along the bark network) on solute fluxes out of the stem. The formulation of stemflow as a directed network problem also opens up the possibility of using percolation theory, where certain precipitation regimes can lead to 'order-disorder' type phase

transition (intermittent versus continuous stem flow into the soil) with critical exponents to be derived from the bark network topology. This approach is timely given the rapid advances in imaging methods that can map the bark.

Future work will hone in on some of the intricacies not included in this version of the model such as transient dynamics in water and solute movement, spatially variable geometric and physio-chemical properties along the entire bark surfaces [45], antecedent conditions in bark moisture, and pH. We note that while we have captured the correct physical scale for trees, our sample calculations do not yet capture the geometric complexity of furrow networks. We reserve this treatment for future research. Further, while mathematically distinct, stemflow solute transport processes should be examined and modeled for smooth-barked trees. In time, when rigorous and viable models are developed for rough- and smooth-barked tree species, it will be possible to begin linking stemflow inputs per unit infiltration area to biogeochemical cycling in the soil-root system. In tandem, the work here inspires future experiments to be designed (in the lab and field) where the bark physio-chemical properties are to be measured and the mapping of flow lines for differing bark geometry are tracked in time. The class of network models proposed here can then be used to link solute concentration time series output from the stem to hydrological regimes and bark properties.

Acknowledgments

A.M.T. acknowledges the summer support from the University of Delaware through the Unidel Foundation. G.K. acknowledges support from the U.S. National Science Foundation (NSF-AGS-1644382 and NSF-IOS-175489). This work was also supported by JSPS KAKENHI Grant Number JP17KK0159. The code used is available at https://github.com/Louminator/stemflow.

Appendix A. Detailed calculations for one network example

In this appendix, how the system of solute transport equations along with the boundary conditions are solved on one network is illustrated. Using conventional notation [2], the beginning and end of a channel along with the intersection of any two furrows is labelled a node. The sections between nodes are denoted “edges,” though these edges represent a volume. Each edge connecting nodes i and j is called e_{ij}. The example used here is for a moderately complex network with flow starting at two nodes, flowing down two edges, mixing at a single node, and, splitting again into two separate edges. This example corresponds to the network described in Fig. 5(d), recreated here for reference as Fig. 10. The set up of the example is consistent with Section 3.

For convenience, furrows are assumed to be rectangular in cross section with uniform width B (Fig. 11). The water depth is determined from the flow rate per furrow using Eq. (6). The flow rate per furrow is determined from total stemflow and the number of furrows that can be packed along the circumference of the tree, also assumed to be constant. All measured and computed parameters are as in Table 3. Each edge has a length of 10m so that the entire system has a length of 20m.

For $n = 1$, Eq. (19) gives an exact solution to the second-order differential equation for c, the dimensionless relative concentration at location x', $0 \leq x' \leq 1$, with unknown constants A and B. These constants will be calculated for each furrow using a system of equations that accommodate the boundary conditions on the network. Keeping with the established notation above, c_{ij} represents the solution in one edge with its associated unknown coefficients A_{ij} and B_{ij}.

To set up the matrix that will solve for A_{ij} and B_{ij} in each furrow, appropriate equations are found by calculating the boundary conditions for each edge. Let $\mathbb{M}$ be the matrix of boundary condition equation coefficients, $\mathbf{v}$ be the vector of unknowns, A_{ij} and B_{ij}, $1 \leq i, j \leq 5$, and $\mathbf{b}$ be the vector corresponding to the right hand side of the boundary condition equations so that we are solving the equation

$$\mathbb{M}\mathbf{v} = \mathbf{b} \tag{29}$$

for $\mathbf{v}$.

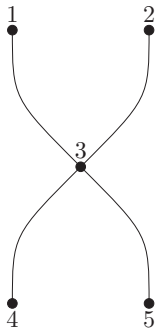

Fig. 10. A moderately complex network for illustrating the calculations of solute transport along a bark.

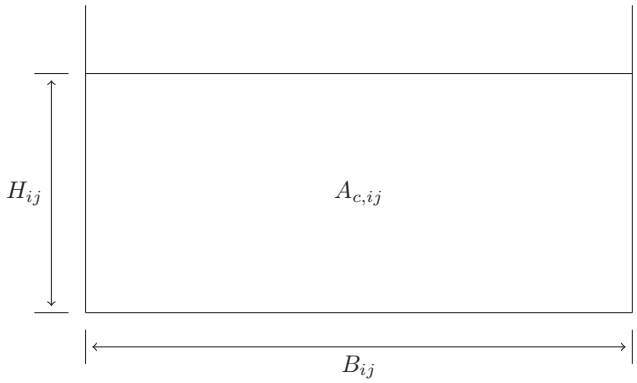

Fig. 11. Cross-section of furrow represented by edge e_{ij}.

The first 2 boundary conditions are the known input at nodes 1 and 2, which we call q_0, so we have in terms of q (the dimensional solute concentration)

$$q_{13}(0) = (q_0/q_R) - 1, \quad \text{and} \quad q_{23}(0) = (q_0/q_R) - 1. \tag{30}$$

Evaluating Eq. (19) at $x = 0$ leads to

$$A_{13} + B_{13} = (q_0/q_R) - 1, \quad \text{and} \quad A_{23} + B_{23} = (q_0/q_R) - 1. \tag{31}$$

For the third boundary condition, the net flux at node 3 must be 0. To find the net flux, we must calculate $\frac{dq}{dx}$ for each edge.

$$\frac{dq}{dx} = q_R\Big[A\underbrace{\frac{1}{2l}\exp\Big(\frac{x}{2l}\Big(\mathrm{Pe}_a - \lambda\Big)\Big)}_{\alpha(x)} + \bar{B}\underbrace{\frac{1}{2l}\exp\Big(\frac{x}{2l}\Big(\mathrm{Pe}_a + \lambda\Big)\Big)}_{\beta(x)}\Big]. \tag{32}$$

In this expression, the constitutive functions $\alpha(x)$ and $\beta(x)$ are not to be confused with the parameters α (angle of incline) and β (asymmetry parameter) used elsewhere in the paper. Recall we are using Eq. (13) to calculate flux, so our general boundary condition is

$$J_{13}|_{x=l_{13}} + J_{23}|_{x=l_{23}} - J_{34}|_{x=0} - J_{35}|_{x=0} = 0, \tag{33}$$

and it simplifies to

$$q_R\Big[dq\alpha_{13}\ \alpha_{13}|_{x=l_{13}} + dq\beta_{13}\ \beta_{13}|_{x=l_{13}} + dq\alpha_{23}\ \alpha_{23}|_{x=l_{23}} + dq\beta_{23}\ \beta_{23}|_{x=l_{23}} - dq\alpha_{34} - dq\beta_{34} - dq\alpha_{35} - dq\beta_{35}\Big] = 0 \tag{34}$$

where

$$\alpha = \frac{1}{2l}\exp\Big(\frac{x}{2l}\Big(\mathrm{Pe}_a - \lambda\Big)\Big), \tag{35a}$$

$$\beta = \frac{1}{2l}\exp\Big(\frac{x}{2l}\Big(\mathrm{Pe}_a + \lambda\Big)\Big), \tag{35b}$$

$$dq\alpha = u - \frac{D}{2l}\Big(Pe_a - \lambda\Big), \tag{35c}$$

and

$$dq\beta = u - \frac{D}{2l}\Big(Pe_a + \lambda\Big). \tag{35d}$$

For the fourth, fifth, and sixth boundary conditions, we use continuity of concentration at node 3, i.e.

$$q_{13}|_{x=l_{13}} - q_{23}|_{x=l_{23}} = 0, \tag{36}$$

$$q_{13}|_{x=l_{13}} - q_{34}|_{x=0} = 0, \tag{37}$$

and

$$q_{13}|_{x=l_{13}} - q_{35}|_{x=0} = 0. \tag{38}$$

Table 4
Results from solving Eq. (29).

A_{13}	−1.00000000e+00
B_{13}	−2.74205488e−18
A_{23}	−1.00000000e+00
B_{23}	−2.74205488e−18
A_{24}	−3.05286378e−01
B_{24}	0.00000000e+00
A_{25}	−3.05286378e−01
B_{25}	0.00000000e+00

Finally, for boundary conditions 7 and 8, we use Robin boundary conditions to account for the outflow at nodes 4 and 5 as below

$$\beta_{34}|_{x=l_{34}} = 0 \tag{39}$$

and

$$\beta_{35}|_{x=l_{35}} = 0. \tag{40}$$

Now that all the boundary conditions are in place, we can solve the system of equations numerically. The results we found are listed in Table 4.

We note that the values of B_{13} and B_{23}, relative to A_{13} and A_{23} respectively, are below machine precision and can be taken to be zero.

References

[1] D. Carlyle-Moses, S. Iida, S. Germer, P. Llorens, B. Michalzik, K. Nanko, A. Tischer, D. Levia, Expressing stemflow commensurate with its ecohydrological importance, Adv. Water Resour. 121 (2018) 472–479, doi:10.1016/j.advwatres.2018.08.015.
[2] L. Heaton, E. López, P. Maini, M. Fricker, N. Jones, Advection, diffusion, and delivery over a network, Phys. Rev. E – Stat. Nonlinear Soft Matter Phys. 86 (021905) (2012), doi:10.1103/PhysRevE.86.021905.
[3] J. Banavar, A. Maritan, A. Rinaldo, Size and form in efficient transportation networks, Nature 399 (6732) (1999) 130–132.
[4] L.D.T. Câmara, A.J.S. Neto, Network modeling of chromatography by stochastic phenomena of adsorption, diffusion and convection, Appl. Math. Model. 33 (5) (2009) 2491–2501.
[5] G. García-Ros, I. Alhama, J.L. Morales, Numerical simulation of nonlinear consolidation problems by models based on the network method, Appl. Math. Model. 69 (2019) 604–620.
[6] D. Ni, J.D. Leonard II, A simplified kinematic wave model at a merge bottleneck, Appl. Math. Model. 29 (11) (2005) 1054–1072.
[7] J. Aboal, D. Morales, M. Hernández, M. Jiménez, The measurement and modelling of the variation of stemflow in laurel forest in Tenerife, Canary Islands, J. Hydrol. 221 (1999) 161–175, doi:10.1016/S0022-1694(99)00086-4.
[8] D. Levia, S. Germer, A review of stemflow generation dynamics and stemflow-environment interactions in forests and shrublands, Rev. Geophys. 53 (2015) 6377–6714, doi:10.1002/2015RG000479.
[9] S. Herwitz, Raindrop impact and water flow on the vegetative surfaces of trees and the effects on stemflow and throughfall generation, Earth Surf. Processes Landforms 12 (1987) 425–432, doi:10.1002/esp.3290120408.
[10] J. Brown, A. Barker, An analysis of throughfall and stemflow in mixed oak stands, Water Resour. Res. 6 (1970) 316–323, doi:10.1029/WR006i001p00316.
[11] D. Dunkerley, Stemflow on the woody parts of plants: dependence on rainfall intensity and event profile from laboratory simulations, Hydrol. Processes 28 (22) (2014) 5469–5482.
[12] D. Levia, Winter stemflow leaching of nutrient-ions from deciduous canopy trees in relation to meteorological conditions, Agric. For. Meteorol. 117 (2003) 39–51, doi:10.1016/S0168-1923(03)00040-6.
[13] C. Cayuela, P. Llorens, E. Sánchez-Costa, D. Levia, J. Latron, Effect of biotic and abiotic factors on inter and intra-event variability in stemflow rates in oak and pine stands in a mediterranean mountain area, J. Hydrol. 560 (2018) 396–406, doi:10.1016/j.jhydrol.2018. 03.050.
[14] G. Parker, Throughfall and stemflow in the forest nutrient cycle, Adv. Ecol. Res. 13 (1983) 57–133, doi:10.1016/S0065-2504(08)60108-7.
[15] K. Kuraji, T. Yuri, T. Nobuaki, K. Isamu, Generation of stemflow volume and chemistry in a mature Japanese cypress forest, Hydrol. Processes 15 (2001) 1967–1978, doi:10.1002/hyp.250.
[16] J. Leff, P. Del Tredici, W. Friedman, N. Fierer, Spatial structuring of bacterial communities within individual Ginkgo biloba trees, Environ. Microbiol. 17 (2015) 2352–2361, doi:10.1111/1462-2920.12695.
[17] D. Levia, J. van Stan, C. Siegert, S. Inamdar, M. Mitchell, S. Mage, P. McHale, Atmospheric deposition and corresponding variability of stemflow chemistry across temporal scales in a mid-atlantic broadleaved deciduous forest, Atmos. Environ. 45 (2011) 3046–3054, doi:10.1016/j.atmosenv.2011.03.022.
[18] H. Mo, M. Bai, D. Lin, J.-C. Roegiers, Study of flow and transport in fracture network using percolation theory, Appl. Math. Model. 22 (4–5) (1998) 277–291.
[19] N. Imamura, D. Levia, J. Toriyama, M. Kobayashi, K. Nanko, Stemflow-induced spatial heterogeneity of radiocesium concentrations and stocks in the soil of a broadleaved deciduous forest, Sci. Total Environ. 599 (2017) 1013–1021.
[20] D. Levia, S. Herwitz, Interspecific variation of bark water storage capacity of three deciduous tree species in relation to stemflow yield and solute flux to forest soils, Catena 64 (2005) 673–714, doi:10.1002/2015RG000479.
[21] G. Gioia, F. Bombardelli, Scaling and similarity in rough channel flows, Phys. Rev. Lett. 88 (1) (2001) 014501.
[22] G. Katul, D. Li, C. Manes, A primer on turbulence in hydrology and hydraulics: the power of dimensional analysis, Wiley Interdiscip. Rev. 6 (2) (2019) e1336.
[23] A.d. Saint-Venant, Theorie du mouvement non permanent des eaux, avec application aux crues des rivieres et al introduction de marees dans leurs lits, Comptes Rendus des Seances de Academie desSciences 36 (1871) 174–154.
[24] M. Melis, D. Poggi, G. Fasanella, D. Oscar, S. Cordero, G. Katul, Resistance to flow on a sloping channel covered by dense vegetation following a dam break, Water Resour. Res. 55 (2) (2019) 1040–1058.
[25] R. Manning, On the flow of water in open channels and pipes transactions, Inst. Civ. Eng. 24 (1895) 179–207.
[26] G. Brown, The history of the Darcy-Weisbach equation for pipe flow resistance, Environ. Water Resour. History 38 (7) (2002) 34–43.
[27] M. LaViolette, On the history, science, and technology included in the Moody diagram, J. Fluids Eng. 139 (3) (2017) 030801.
[28] L. Moody, Friction factors for pipe flow, Trans. Am. Soc. Mech.Eng. 66 (1944) 671–684.

[29] G. Gioia, P. Chakraborty, Turbulent friction in rough pipes and the energy spectrum of the phenomenological theory, Phys. Rev. Lett. 96 (4) (2006) 044502.
[30] B. McKeon, C. Swanson, M. Zagarola, R. Donnelly, A. Smits, Friction factors for smooth pipe flow, J. Fluid Mech. 511 (2004) 41–44.
[31] M. Scholle, N. Aksel, An exact solution of visco-capillary flow in an inclined channel, Z. Angew. Math. Phys.ZAMP 52 (2001) 749–769, doi:10.1007/PL00001572.
[32] M. Scholle, N. Aksel, Thin film limit and film rupture of the visco-capillary gravity-driven channel flow, Z. Angew. Math. Phys.ZAMP 54 (2003) 517–531, doi:10.1007/s00033-003-2090-z.
[33] S. Bonetti, G. Manoli, C. Manes, A. Porporato, G. Katul, Mannings formula and stricklers scaling explained by a co-spectral budget model, J. Fluid Mech. 812 (2017) 1189–1212.
[34] G.I. Taylor, Dispersion of soluble matter in solvent flowing slowly through a tube, Proc. R. Soc. Lond. Ser.A 219 (1137) (1953) 186–203.
[35] S. Chikwendu, Calculation of longitudinal shear dispersivity using an N-zone model as $N \rightarrow \infty$, J. Fluid Mech. 167 (1986) 19–30.
[36] G.I. Taylor, The dispersion of matter in turbulent flow through a pipe, Proc. R. Soc. Lond. Ser.A 223 (1155) (1954) 446–468.
[37] H. Fischer, Longitudinal dispersion and turbulent mixing in open-channel flow, Annu. Rev. Fluid Mech. 5 (1) (1973) 59–78.
[38] L. Segel, L. Edelstein-Keshet, A Primer on Mathematical Models in Biology, Society for Industrial and Applied Mathematics, Philadelphia, PA. doi:10.1137/1.9781611972504.
[39] Z. Neufeld, P. Haynes, T. Tél, Chaotic mixing induced transitions in reaction–diffusion systems, Chaos 12 (2) (2002) 426–438.
[40] T. Tél, A. de Moura, C. Grebogi, G. Károlyi, Chemical and biological activity in open flows: adynamical system approach, Phys. Rep. 413 (2–3) (2005) 91–196.
[41] L. Puckett, Time-and pH-dependent leaching of ions from deciduous and coniferous foliage, Can. J. For. Res. 20 (11) (1990) 1779–1785.
[42] A. Carlisle, A. Brown, E. White, The nutrient content of tree stem flow and ground flora litter and leachates in a sessile oak (*quercus petraea*) woodland, J. Ecol. (1967) 615–627.
[43] L. Gosting, A study of the diffusion of potassium chloride in water at 25° with the Gouy interference method, J. Am. Chem. Soc. 72 (1950) 4418–4422, doi:10.1021/ja01166a021.
[44] D. Levia, J. Van Stan II, S. Mage, P. Kelley-Hauske, Temporal variability of stemflow volume in a beech-yellow poplar forest in relation to tree species and size, J. Hydrol. 380 (1–2) (2010) 112–120.
[45] S. Köhler, D. Levia, H. Jungkunst, G. Gerold, An in situ method to measure and map bark ph, J. Wood Chem. Technol. 35 (6) (2015) 438–449.